Article

Taming the natural boundary of centered polygonal lacunary functions: Restriction to the symmetry angle space

L.K. Mork [1], Keith Sullivan [2] and Darin J. Ulness [2,*]

[1] Department of Mathematics, Concordia College, Moorhead, MN 56562, USA
[2] Department of Chemistry, Concordia College, Moorhead, MN 56562, USA
* Correspondence: ulnessd@cord.edu

Abstract: This work investigates centered polygonal lacunary functions restricted from the unit disk onto symmetry angle space which is defined by the symmetry angles of a given centered polygonal lacunary function. This restriction allows for one to consider only the p-sequences of the centered polygonal lacunary functions which are bounded, but not convergent, at the natural boundary. The periodicity of the p-sequences naturally gives rise to a convergent subsequence, which can be used as a grounds for decomposition of the restricted centered polygonal lacunary functions. A mapping of the unit disk to the sphere allows for the study of the line integrals of restricted centered polygonal that includes analytic progress towards closed form representations. Obvious closures of the domain obtained from the spherical map lead to four distinct topological spaces of the "broom topology" type.

Keywords: Lacunary function, Gap function, Centered polygonal numbers, Natural boundary, Singularities, Broom topology

---

1. Introduction

Lancunary functions are a special class of analytic functions whose singularities coalesce into a curve called a natural boundary [1,2] (as opposed to the more commonly studied meromorphic functions having isolated singularites). Lacunary functions are those whose power series is characterized by "gaps" (or "lacunae") in the progression of terms. Because the natural boundary is difficult to deal with, functions with natural boundaries have not seen extensive use in physics over the years. Nonetheless, lacunary functions have found some recent use in tackling physical problems in quantum mechanics [3,4], optics [5], and statistical mechanics [6–9].

Of the lacunary functions, the family generated by centered polygonal numbers have particularly interesting features. This family is called centered polygonal lacunary functions. Their special properties are mainly due to the unusual symmetry present in this family, compared to an arbitrary lacunary function [10–12]. A class of infinite sequences associated with lacunary functions are called lacunary sequences and recent work has focused on exploring particular bounded sequences of numbers arising at the natural boundary of centered polygonal lacunary sequences [10,11]. These p-sequences, as they are called, have been well characterized and this work has been significantly enhanced by the construction of graphs to represent the p-sequences [10]. The graphs that have arisen are interesting in and of themselves, especially in that they reveal self-similarity and scaling that allow for a renormalization approach [11]. The self-similarity hints at the fractal character of the centered polygonal lacunary functions. Indeed, explicit investigation of this fractal character in the form of Julia sets has recently been presented [12].

This current contribution builds upon the above mentioned work and is focused on some of the substructure in the summation terms of the centered polygonal lacunary functions as well as the behavior of these functions on restricted subspaces of the unit disk. The periodic nature of the p-sequences and the fact that there is a well-defined sequence that actually converges to zero at the natural boundary offers an opportunity to make some degree of sense of the centered polygonal lacunary functions at the natural boundary. This is the case, at least, when restricting the domain from the unit disk onto a set of line segments which are determined by the function itself. This restricted space is referred to here as the symmetry angle space and is defined in Section 4. Symmetry angle space, as a topology, is very much like the so-called "broom topology" [13]. The periodic nature of the p-sequences suggests a natural decomposition of the centered polygonal lacunary functions on symmetry angle space.

Further, there is a convenient surjective mapping of the unit disk to the sphere such that the natural boundary maps to a single point. Symmetry angle space then consists of the union of longitudinal lines on S^2. Obvious closures of the mapped symmetry angle space allow inclusion of the natural boundary as a single point. Line integrals are investigated which include loops "through" the natural boundary.

The ultimate goal of the current work is to provide some useful insight into the nature of the natural boundary of centered polygonal lacunary functions.

2. Centered polygonal lacunary functions

Definitions, notation, and some theorems from references [10] and [11] are briefly collected here for the convenience of the reader.

The N^{th} member of a lacunary sequence of functions is defined here as

$$f_N(z) = \sum_{n=1}^{N} z^{g(n)}, \tag{1}$$

where $g(n)$ is a function of n that follows the criteria of Hadamard's gap theorem [2]. (Note that the sum starts at $n = 1$ for convenience but not necessity.) Following references [10,11], we use the notation

$$\mathfrak{L}(g;z) \equiv \left\{ f_N(z) = \sum_{n=1}^{N} z^{g(n)} \right\}, \tag{2}$$

to represent the particular lacunary sequence described by $g(n)$, in complex variable z. For one example, $\mathfrak{L}(\frac{n(n+1)}{2};z) \equiv \left\{ f_N(z) = \sum_{n=1}^{N} z^{\frac{n(n+1)}{2}} \right\}$. The lacunary function associated with the sequence $\mathfrak{L}(\frac{n(n+1)}{2};z)$ is $f(z) = \lim_{N\to\infty} f_N(z)$. One particularly important representation of this example function is shown in the bottom left panel of Fig. 1.

A $g(n)$ family of note that yields particularly interesting lacunary functions are the centered polygonal numbers. The centered polygonal numbers are a sequence of numbers arising from considering points on an polygonal lattice [14–17]. The centered k-gonal numbers are defined by the formula

$$C^{(k)}(n) = \frac{kn^2 - kn + 2}{2}, \quad n \geq 1. \tag{3}$$

When $g(n) = C^{(k)}(n)$ is the n^{th} centered k-gonal number, then $f(z) = \sum_{n=1}^{\infty} z^{C^{(k)}(n)}$ is the centered polygonal lacunary function. Also, $\mathfrak{L}(C^{(k)};z)$ is the centered polygonal lacunary sequence associated with f.

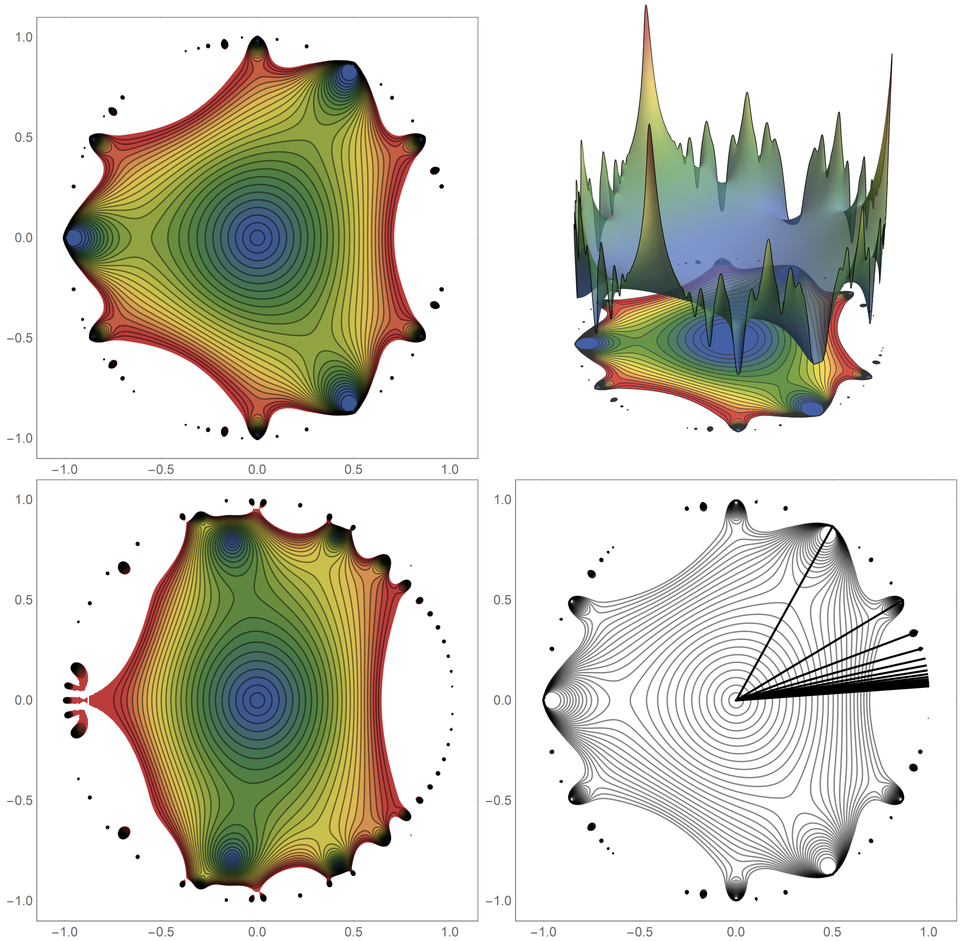

Figure 1. A particularly illustrative way to present graphs of $\mathfrak{L}(C^{(k)};z)$. The representation shown here is especially useful for this work. The contour plot is truncated at the unity level set (blue shading represents low values and red shading represents high values). The top left panel shows the example of $\mathfrak{L}(C^{(3)};z)$ where a plot of $|f_{16}(z)|$. The top right panel shows a superposition of the contour plot and a three-dimensional rendering. The truncated contour plot more clearly exposes the true rotational symmetry of the centered polygonal lacunary functions. The bottom left graphs shows the case of $\mathfrak{L}(T_n;z)$ again for $|f_{16}(z)|$. Despite the intimate relationship between the centered polygonal numbers and the triangular numbers, the plots are strikingly different. The bottom right panel shows an unshaded contour plot of the same function shown in the left panel of Fig. 1. The superimposed black lines indicate the symmetry angles. The first 15 symmetry angles are shown (see text for details).

It turns out that nearly all of the structural features of centered polygonal lacunary functions are independent of the choice of k [10,11]. This is because the centered polygonal numbers are related to the triangular numbers [18] in a simple way. The set of triangular numbers is

$$T = \left\{ \frac{n(n+1)}{2} \right\}. \tag{4}$$

For convenience, lemmas, theorems, and corollaries are proven in reference [10] are stated here without proof. A couple of definitions from reference [10] are included as well.

Lemma 2.1.
$$\frac{C^{(k)}(n+1)-1}{k} = T(n), \tag{5}$$
where $C^{(k)}(n)$ and $T(n)$ mean the n^{th} member of the respective sets.

Lemma 2.2. *The sequence of triangular numbers mod p is a $2p$-cycle. The sequence is symmetric about the midpoint of the $2p$-cycle. The $2p^{th}$ member of the $2p$-cycle is zero.*

Lemma 2.3. *There is an equal number of even and odd numbers in the first p members of $2p$-cycle of lemma 2.2.*

Theorem 2.4. *All values appear once and only once in the first p members of the $2p$-cycle if and only if $p = 2^m$ where m is a positive integer.*

Corollary 2.5. *If $p \neq 2^m$ then the first time 0 appears is at a position less than the $p-1$ position. The converse is also true.*

Theorem 2.6. *Values appear no more than twice in the first p members of the $2p$-cycle for p prime.*

Definition 2.1. *Primary symmetry. The rotational symmetry of the $N = 2$ member of $|\mathfrak{L}(g;z)|$, $|f_2(z)|$, is called the* primary symmetry.

Theorem 2.7. *The primary symmetry of $|\mathfrak{L}(g(n);z)|$ is $k = g(2) - g(1)$.*

3. The p-sequences

The centered polygonal lacunary functions have very interesting organizational structure at the natural boundary [10,11]. Of particular interest are the p-sequences [10]. These arise when considering the value of the centered polygonal lacunary function on the line segment that runs from the origin to the natural boundary at an angle of $\phi = \frac{\pi}{kp}$, $p \in \mathbb{Z}^+$. Interestingly, in the limit of $\rho \to 1_-$, the sequence $\mathfrak{L}\left(C^{(k)}; \rho e^{\frac{i\pi}{kp}}\right)$ becomes a bounded $4p$ cycle of complex numbers [10].

Definition 3.1. *Symmetry angle. Let the primary symmetry be k-fold. The* first symmetry angle *is $\alpha_p = \frac{\pi}{k}$, $k \in \mathbb{Z}$. The p^{th} symmetry angle is $\alpha_p = \frac{\pi}{pk}$, $p, k \in \mathbb{Z}$. The* primary symmetry angle *is α_1.*

At the natural boundary, the p-sequences have intricate structure [10] that is a manifestation of Lemma 2.1. Because of Lemma 2.2, the values of $f_N(e^{i\alpha_p})$, although not convergent, do not diverge; they simply oscillate. Further, they take on the value of zero at values of $N = 4mp$. This allows for a convergent sub-sequence which is discussed in Section 5.

This section concludes with an additional theorem specific to centered polygonal numbers proven here.

Theorem 3.1. *The following rearrangement holds for $f_N(\rho e^{i\alpha_p})$.*

$$f_N(\rho e^{i\alpha_p}) = \sum_{n=1}^{N} (\rho e^{\frac{i\pi}{kp}})^{C^k(n)} = \sum_{n=1}^{N} (-1)^{\left\lfloor \frac{C^{(k)}(n)}{kp} \right\rfloor} (-1)^{\frac{C^{(k)}(n) \mod (kp)}{(kp)}} \rho^{C^{(k)}(n)}, \tag{6}$$

where $\lfloor x \rfloor$ indicates the floor function.

Proof. Inspection shows that it will suffice to show

$$(e^{\frac{i\pi}{kp}})^{C^k(n)} = (-1)^{\left\lfloor \frac{C^{(k)}(n)}{kp} \right\rfloor} (-1)^{\frac{C^{(k)}(n) \mod (kp)}{(kp)}}. \tag{7}$$

Beginning by expressing $e^{i\pi}$ as -1, one has

$$(e^{\frac{i\pi}{kp}})^{C^{(k)}(n)} = e^{\frac{i\pi C^{(k)}(n)}{kp}} = e^{i\pi \frac{C^{(k)}(n)}{kp}} = (e^{i\pi})^{\frac{C^{(k)}(n)}{kp}} = (-1)^{\frac{C^{(k)}(n)}{kp}} \tag{8}$$

Now, one wants to separate the integer part of $\frac{C^{(k)}(n)}{kp}$ from the fractional part because of the modularity of $(-1)^x$. To that end, $C^{(k)}(n)$ can be written as $m(kp) + r$, where $m = \left\lfloor \frac{C^{(k)}(n)}{kp} \right\rfloor$ and $r = C^{(k)}(n) \mod (kp)$. From $(-1)^{\frac{m(kp)+r}{kp}} = (-1)^m(-1)^{\frac{r}{kp}}$, one has Eq. (7). Thus Eq. (6) holds and Theorem 3.1 is proven. □

This theorem has real practical use in that it radically speeds up certain calculations and simplifies certain expressions on MATHEMATICA.

4. Symmetry angle spaces

The focus of this work is to restrict the centered polygonal functions, which are analytic on the open complex disk, to a topological space consisting of the union of the line segments lying along the symmetry angles which run from the origin to the natural boundary (located on the unit circle)

Let $\mathcal{D}$ be the open unit disk in the complex plane and let let $\bar{\mathcal{D}}$ be the closed unit disk. Further, one can define $\mathcal{I}_p \equiv \rho e^{\frac{i\pi}{kp}}$ for $0 \le \rho < 1$ (that, is the line segment along the p^{th} symmetry angle, α_p. One likewise define the closure of $\mathcal{I}_p$ as $\bar{\mathcal{I}}_p$, where now $0 \le \rho \le 1$.

The symmetry angle space is then defined as

$$\mathcal{P} \equiv \bigcup_{p=1}^{\infty} \mathcal{I}_p, \tag{9}$$

and its closure,

$$\bar{\mathcal{P}} \equiv \bigcup_{p=1}^{\infty} \bar{\mathcal{I}}_p \tag{10}$$

Note that as p approaches ∞ the symmetry line approaches the real axis. Thus one needs to consider a second type of closure. If the real line is included, one denotes the subspaces as $\check{\mathcal{P}}$ and $\check{\bar{\mathcal{P}}}$.

Thus there are four related subspaces upon which the centered lacunary functions are restricted: $\mathcal{P}$, $\bar{\mathcal{P}}$, $\check{\mathcal{P}}$, and $\check{\bar{\mathcal{P}}}$. These subspaces are related to the so-called broom topological spaces [13]. They naturally take on a subspace topology, that is the normal topology for a line segment. All four of these subspaces are arc-connected and, in fact, star-connected through the origin. In Section 7, $\mathcal{P}$, $\bar{\mathcal{P}}$, $\check{\mathcal{P}}$, and $\check{\bar{\mathcal{P}}}$ are homeomorphically mapped to longitudinal lines of the sphere. This allows for closed form expressions for integrals of $f(z)$ along paths in these mapped spaces.

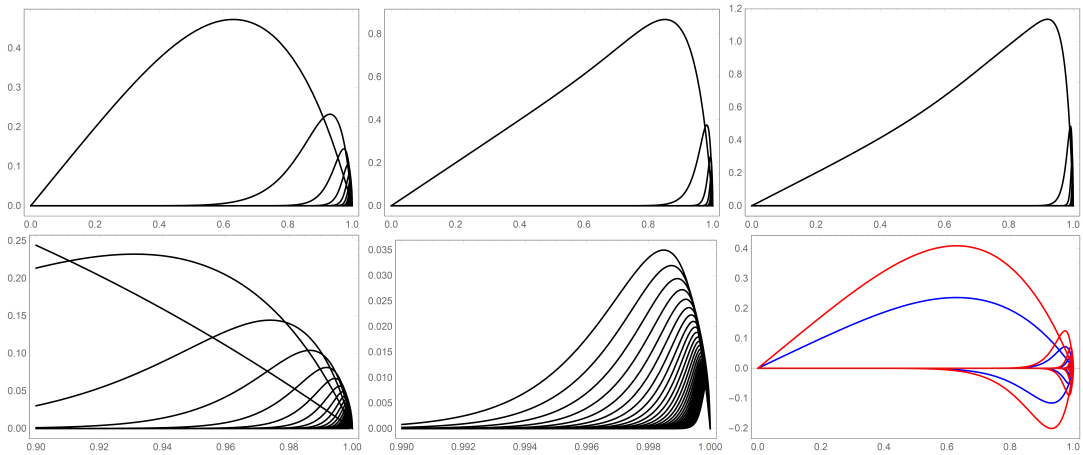

Figure 2. Cyclic decompositions for the centered polygonal lacunary functions along three of the line segments shown in the bottom right panel of Fig. 1, *i.e.*, $k = 3$. The first 40 f_j are shown. The top row shows $|f_{40p}(\rho e^{\frac{i\pi}{3p}})|$: left panel $p = 1$, middle panel $p = 2$, right panel $p = 3$. The bottom row focuses on the $p = 1$ case in more detail. The left and middle panels show a sequential blow up near the natural boundary of the top left graph (note the displayed domain on the ρ axis). For better clarity, the first 10 f_j are not shown in the left panel and the first 20 f_j are not shown in the middle panel. Finally, the bottom right panel shows the real (blue) and imaginary (red) parts of $f_{40}(\rho e^{\frac{i\pi}{3}})$, *i.e.*, $k = 3$, $p = 1$.

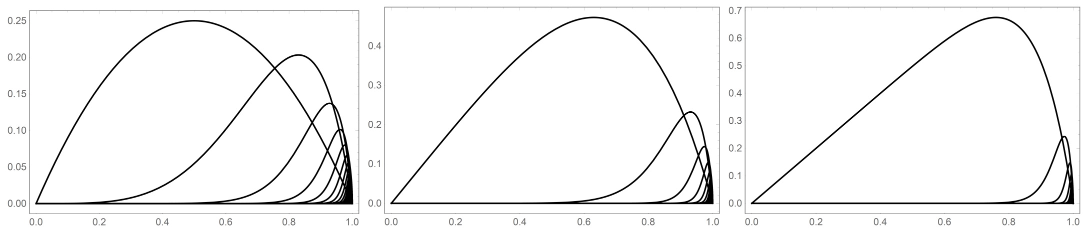

Figure 3. Cyclic decompositions for the centered polygonal lacunary functions along the line segments at α_1 for (left-to-right) $k = 1$, $k = 3$ (sames as in Fig. 2), and $k = 8$. The other parameters are the same as in Fig. 2. Increasing k skews the graph towards the natural boundary.

5. Cyclic decomposition

Along the symmetry angle, the resultant p-sequence has a $4p$ cycle, and, in fact, the $4p$ cycle further breaks into a $2p$-cycle at the modulus level as discussed in Section 3. Finally, by Lemma 2.2 the $2p^{\text{th}}$ member of the the $2p$ cycle is zero. Because of this, it is natural to consider a subset of $\mathfrak{L}\left(C^{(k)}, \rho e^{\frac{i\pi}{kp}}\right)$ for which $N = 2pm$, $m \in \mathbb{Z}^+$; call this subsequence $\hat{\mathfrak{L}}\left(C^{(k)}, \rho e^{\frac{i\pi}{kp}}\right)$. For every member of this subsequence $\lim_{\rho \to 1_-}$ is zero.

One can express the j^{th} cycle as

$$f_j^{(k)}(\rho e^{\frac{i\pi}{kp}}) = \sum_{pj+1}^{2p(j+1)} \rho e^{\frac{i\pi}{kp}}, \tag{11}$$

where $j \geq 0 \in \mathbb{Z}$. Thus, the full function can be decomposed into the cyclic summations,

$$f^{(k)} = \sum_{j=1}^{\infty} f_j^{(k)}. \tag{12}$$

Figure 2 shows the cyclic summation decomposition of $f^{(3)}(\rho e^{\frac{i\pi}{3p}})$ for the examples of $p = 1$ and $p = 3$. The fundamental component, $f_0^{(3)}$, captures much of the full function, but deviates significantly

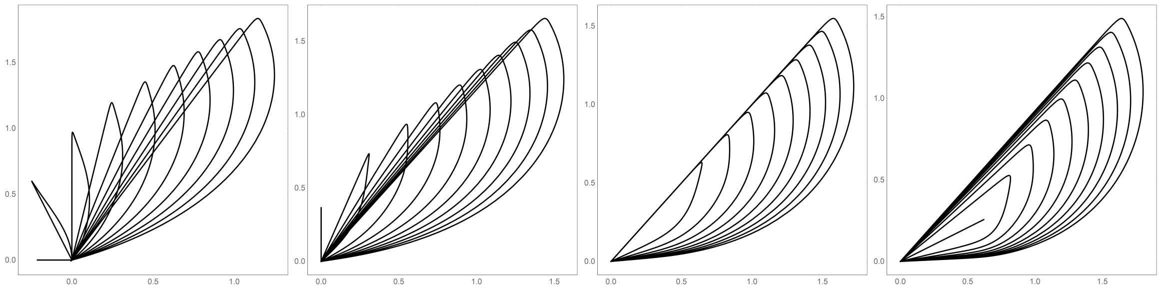

Figure 4. Parametric curves, $\mathsf{P}^{(3)}(\rho; p)$ from Eq. (13), of $f_N(z)$ for four different values of k read left-to-right, top-to-bottom: $k = 1$, $k = 2$, $k = 4$, $k = 8$. Shown are the first 10 values of p. The case of $p = 1$ has no interior points and is directed at an angle equal to α_1 in $\mathbb{R}^2$. Increasing values of p lead to closed curves which are bigger and have greater interior area. As ρ goes from 0 to 1 the curve is traversed in a counterclockwise direction.

as $\rho \simeq 0.9$. The actual peak occurs at $\rho = \rho_{\max}$. Inspection of Fig. 2 shows that $\rho_{\max}$ increases with increasing k as the curves are skewed towards the natural boundary.

The higher components $j \geq 1$ contribute very little for low values of ρ. Each of the subsequent higher components begin to make significant contributions to the full function closer and closer to the natural boundary. One notices in Fig. 2 that both the real (blue curve in figure) and imaginary (red curve) parts of the component cyclic summations alternate signs.

6. Parametric curves

The centered polygonal lacunary functions on $\mathcal{P}$ can be represented in a visually instructive way via the parametric curves:

$$\mathsf{P}^{(k)}(\rho; p) = \left(\mathrm{Re}\left[f^{(k)}(\rho e^{\frac{i\pi}{kp}}) \right], \mathrm{Im}\left[f^{(k)}(\rho e^{\frac{i\pi}{kp}}) \right] \right). \tag{13}$$

The parametric curves for $k = 1, 2, 4, 8$ are shown in Fig. 4. Here values of $p \in \{1, ..., 10\}$ are shown for each k. (Note, $\mathsf{P}^{(k)}$ is plotted in an auxiliary $\mathbb{R}^2$ plane, not in the original complex plane containing $\mathcal{P}$.)

The most obvious feature is that these produce a closed curve in the plane starting at the origin for $\rho = 0$ and returning to the origin for $\rho = 1$. Note that the curves $\mathsf{P}^{(k)}(\rho; 1)$ are all degenerate meaning that the encircled area is zero. Higher values of p give rise to larger and larger enclosed areas (Fig. 4). Hand-in-hand with increasing area is increasing arclength which is also shown in Figs. 4 and 5.

A more subtle view of the closed curves reveals an "acceleration" with ρ and this acceleration increases with increasing p. The "velocity" is represented as red tangent vectors in Fig. 5. One notices a slow acceleration along the lower arc of the curve (for $\rho < \rho_{\max}$). Acceleration then rapidly increases at the apex of the curve and along the return path ($\rho \geq \rho_{\max}$). The change in acceleration at the apex corresponds to an abrupt change in arclength with ρ (see the bottom left panel of 5). An incidental observation regarding arclength is that it closely fits an empirical curve of the from $h(p) = A\sqrt{p} + c$ regardless of k (see bottom right panel of Fig. 5).

Perhaps more interesting, however, is the geometrical behavior of the curves. The initial angle of the curve at $\rho = 0$ is $\alpha_p = \frac{\pi}{kp}$. This is intuitive and quick to prove.

Theorem 6.1. *The initial angle of* $\mathsf{P}^{(k)}(\rho; p)$ *is* α_p.

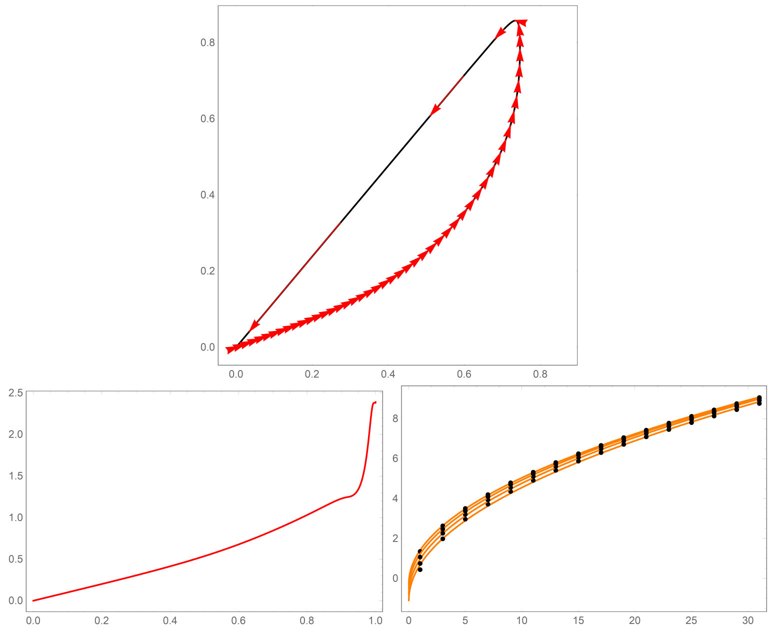

Figure 5. Top: Parametric plot $\mathsf{P}^{(3)}(\rho;p)$ (black curve) superimposed with red vectors indicating the "velocity" along the curve. One notices a modest "acceleration" until the curve turns back towards the origin whereupon the acceleration is markedly increased. Bottom left: the arclength (ordinate) versus ρ (abscissa) for $\mathsf{P}^{(3)}(\rho;p)$. Bottom right: Arclength of $\mathsf{P}^{(k)}(\rho;p)$ for $p=1$–$p=30$ (black dots) associated with the parametric plots shown in Fig. 4 fitted to $A\sqrt{p}+c$ (orange curve). The top curve is for $k=1$ and the bottom curve is for $k=8$. Fit parameters (A,c) for $k=1$, $k=2$, $k=4$, $k=8$ respectively: $(1.7880,-1.1038)$, $(1.7571,-0.7926)$, $(1.7175,-0.5052)$, $(1.6794,-0.2701)$.

Proof. One can make use of the fact that for small ρ, $f_N(z)$ is dominated by the first term in the sum. This goes as

$$\lim_{\rho\to 0} f_N^{(k)}(\rho e^{\frac{i\pi}{kp}}) = \lim_{\rho\to 0}\sum_{n=1}^{N}(\rho e^{\frac{i\pi}{kp}})^{\mathsf{C}^{(k)}(n)} \sim \rho e^{\frac{i\pi}{kp}}. \tag{14}$$

The asymptoptic form follows from the fact that $\mathsf{C}^{(k)}(1)=1$. The phase is clearly $\frac{i\pi}{kp}=\alpha_k$, which completes the proof. □

Less intuitive is the behavior of the return angle as $\rho\to 1_-$. First after $\rho_{\max}$ the curve is nearly a straight line. Further, the angle of that line is $\frac{\pi}{k}$ for $p=1$, but, interestingly, it asymptotically goes to $\frac{\pi}{4}$ as $p\to\infty$. The return angle becomes independent of k. The proof of this statement is probabilistic in nature and is wanting of a more rigorous proof.

Theorem 6.2. *The return angle of* $\mathsf{P}^{(k)}(\rho;p)$ *for* $p=1$ *is* $\frac{\pi}{k}$.

Proof. From Theorem 3.1 and $p=1$, one has

$$f_N(\rho e^{i\alpha_1}) = \sum_{n=1}^{N}(-1)^{\left\lfloor \frac{\mathsf{C}^{(k)}(n)}{k}\right\rfloor}(-1)^{\frac{\mathsf{C}^{(k)}(n) \mod k}{k}}\rho^{\mathsf{C}^{(k)}(n)}. \tag{15}$$

Now,

$$\left\lfloor \frac{C^{(k)}(n)}{k} \right\rfloor = \left\lfloor \frac{kn^2 - kn + 2}{2k} \right\rfloor = \left\lfloor \frac{n^2 - n}{2} + \frac{1}{k} \right\rfloor$$
$$= \left\lfloor \frac{n^2 - n}{2} \right\rfloor = m(n) \in \mathbb{N} \tag{16}$$

and

$$\frac{C^{(k)}(n) \mod k}{k} = \frac{1}{k}\left(\frac{kn^2 - kn + 2}{2} \mod k\right)$$
$$= \frac{1}{k}\left(\frac{k(n^2 - n)}{2} + 1 \mod k\right)$$
$$= \frac{1}{k}. \tag{17}$$

So this reduces $f_N(\rho e^{i\alpha_1})$ to

$$f_N(\rho e^{i\alpha_1}) = \sum_{n=1}^{N} (-1)^{m(n)} (-1)^{\frac{1}{k}} \rho^{C^{(k)}(n)}$$
$$= (-1)^{\frac{1}{k}} \sum_{n=1}^{N} (-1)^{m(n)} (-1)^{\frac{1}{k}} \rho^{C^{(k)}(n)}. \tag{18}$$

The sum is now pure real and setting $(-1)^{\frac{1}{k}} = e^{\frac{i\pi}{k}}$. Hence, the return angles is $\frac{\pi}{k}$. $\square$

Conjecture 6.3. *In the limit of large p, the return angle of $\mathrm{P}^{(k)}(\rho; p)$ is $\frac{\pi}{4}$.*

Proof. The proof is subtle and an analytic one remains elusive. Nonetheless, the conjecture is understandable on probabilistic grounds. Unfortunately, the limit of $\rho = 1$ is not helpful since the function is identically zero and information about the approach angle is lost. As opposed to the case of $\lim_{\rho\to 0}$, the case of $\lim_{\rho\to 1_-}$ now activates many terms in the summation of $f_N^{(k)}(\rho e^{\frac{i\pi}{kp}})$. In between $\rho_{\max}$ and 1 there is not equal weighting of the terms in the cyclic summation, but the weights of the higher terms are no longer negligible. Thus, the limit is a (non-zero) weighted average of many terms. For large p values, the weighed average of many $C^{(k)}(n)$ ultimately gives rise to $\mathrm{Re}\left[f_N^{(k)}\right] = \mathrm{Im}\left[f_N^{(k)}\right]$ and, hence, the return angle is $\frac{\pi}{4}$. $\square$

Because these parametric curves produce enclosed regions, the area within the curves can be calculated. This area is found through a numerical integration of the curve, however the area of every value of k for $p = 1$ will be zero, as the parametric graph of $p = 1$ is a straight line. Fig. 6 is a graph of the area of the associated parametric curves for $1 \le k \le 5$ and $1 \le p \le 10$. Each set of points shows the area for a distinct k value, with the bottom set being the area of $k = 1$, and the top being the area of $k = 5$. As the p value increases a linear trend appears, however the equation for what p approaches to does not seem to have a general trend.

7. Whole sphere mapping

Due to the natural boundary of the centered polygonal lacunary functions sitting on the unit circle in the complex plane, there is no reason to consider the domain outside of the closed disk. There is an interesting and convenient mapping that maps the disk to S^2 such that the entire unit circle is mapped to the south pole ($(0, 0, -1)$). As will be seen, this, in some sense, compresses the natural boundary to an isolated singularity. Further, the symmetry angle spaces map to longitudinal arcs and, given the nature of the p-sequences, this singularity is, again in some sense, removed.

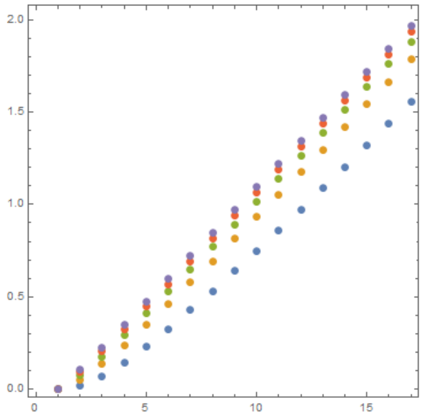

Figure 6. Plot of area verses p value for $1 \leq p \leq 17$ and $1 \leq k \leq 5$. Where the lowest set is the area of $k = 1$ and each successively higher line corresponds to the next greatest k value. The area for each p value approaches to a distinct line for each k value.

The parametric mapping (of S^2 embedded in $\mathbb{R}^3$) is

$$\begin{aligned} &\hat{S} : \bar{\mathcal{D}} \to S^2 \\ &(x, y) \mapsto \left(\cos(\phi)\sin\left(\frac{\theta}{2}\right), \sin(\phi)\sin\left(\frac{\theta}{2}\right), \cos(\theta)\right). \end{aligned} \tag{19}$$

The restriction to, for example, $\bar{\mathcal{P}}$ induces the map

$$\begin{aligned} &\hat{S}_{\bar{\mathcal{P}}} : \bar{\mathcal{D}} \to S^2_{\bar{\mathcal{P}}} \\ &(x, y) \mapsto \left(\cos(\alpha_p)\sin\left(\frac{\theta}{2}\right), \sin(\alpha_p)\sin\left(\frac{\theta}{2}\right), \cos(\theta)\right) \end{aligned} \tag{20}$$

Here $S^2_{\bar{\mathcal{P}}}$ is the restricted domain of longitudinal arcs; an example is shown in Fig. 8. $S^2_{\bar{\mathcal{P}}}$ (as well as $S^2_{\check{\bar{\mathcal{P}}}}$) are star-connected through both the north pole (origin) and south pole (contracted unit circle). Because of this, one can define loops on $S^2_{\bar{\mathcal{P}}}$ and $S^2_{\check{\bar{\mathcal{P}}}}$, with the north pole as the base-point, that traverse one longitudinal arc $S^2_{\bar{\mathcal{I}}_i}$ and return along another $S^2_{\bar{\mathcal{I}}_j}$. The fundamental group (in the homotopy sense) is $\pi_1 = \prod^{\infty} * \mathbb{Z} = \mathbb{Z} * \mathbb{Z} * \cdots$, where $*$ is the loop product.

The spaces $S^2_{\bar{\mathcal{P}}}$ and $S^2_{\check{\bar{\mathcal{P}}}}$ offers an interesting opportunity to explore closed-loop path integrals of $f_N(z)$. Call the path along the p symmetry angle running from the north pole to south pole in $S^2_{\bar{\mathcal{P}}}$, Γ_p. Then a closed-loop can be obtained by considering $\Gamma_{ij} \equiv \Gamma_{p_i} - \Gamma_{p_j}$. The integral along Γ_p is expressed as

$$\begin{aligned} I_p = &\int_0^{\pi} f_N\left(\cos(\alpha_p)\sin\left(\frac{\theta}{2}\right) + i\sin(\alpha_p)\sin\left(\frac{\theta}{2}\right)\right) \\ &\times \frac{(\cos\alpha_p + i\sin\alpha_p)\cos\left(\frac{\theta}{2}\right)}{2} d\theta. \end{aligned} \tag{21}$$

The second factor accounts for the appropriate integration metric along angle α_p. This integral can be evaluated and one has the following theorem.

Theorem 7.1.

$$I_p = e^{\frac{2\pi i}{kp}} \sum_{n=1}^{N=4mp} \frac{(-1)^{\frac{n^2-n}{2p}}}{C^{(k)}(n) + 1}. \tag{22}$$

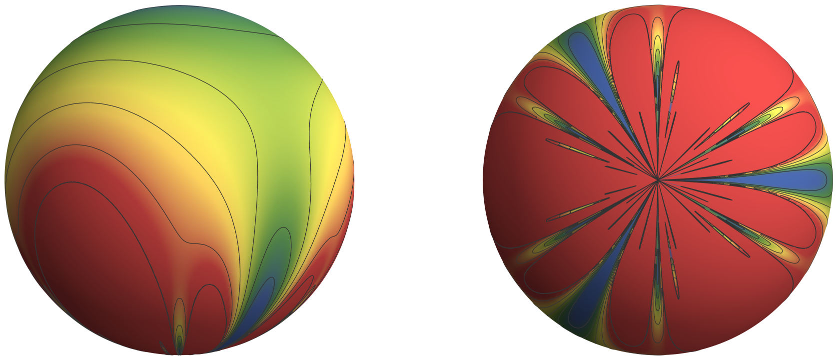

Figure 7. The whole sphere mapping of $\bar{\mathcal{D}}$ onto S^2 (see text for the equations of the map). The mapping is that of the centered polygonal lacunary function shown in Fig. 1 under $\hat{S}$. Two different viewpoints of the same function ($|f_{16}^{(3)}(z)|$) are shown. The left panel shows a "front" view such that the north pole $(0,0,1)$ is located directly on top and the south pole $(0,0,-1)$ directly on the bottom. The right panel shows the "bottom" view such that the south pole is directly in the center of the image. The unit circle maps to the single point at the south pole.

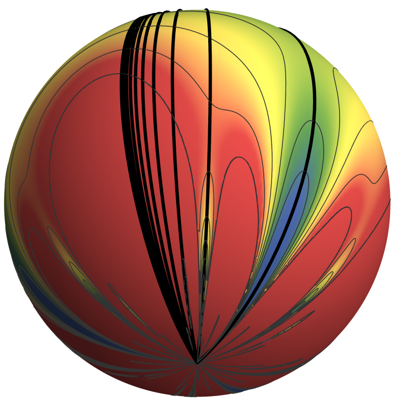

Figure 8. The superposition of the line segments shown in the bottom right panel of Fig. 1 onto the sphere shown in Fig. 7 under the mapping $\hat{S}$.

Proof. Now (writing $\cos\alpha_p + i\sin\alpha_p$ as e^{α_p}), Eq. (21) is

$$I_p = \frac{1}{2}\int_0^\pi f_N\left(e^{i\alpha_p}\sin\left(\frac{\theta}{2}\right)\right)e^{i\alpha_p}\cos\left(\frac{\theta}{2}\right)d\theta. \tag{23}$$

Expressing f_N in summation form and interchanging the summation and the integration gives

$$I_p = \frac{1}{2}\sum_{n=1}^{N=4mp} e^{i\alpha_p(C^{(k)}(n)+1)}\int_0^\pi\left(\sin\left(\frac{\theta}{2}\right)\right)^{C^{(k)}(n)}\cos\left(\frac{\theta}{2}\right)d\theta. \tag{24}$$

Using,

$$\int_0^\pi\left(\sin\frac{\theta}{2}\right)^n\cos\frac{\theta}{2} = \frac{2}{n+1}, \tag{25}$$

the integral is quickly evaluated.

$$\begin{aligned} I_p &= \frac{1}{2}\sum_{n=1}^{N=4mp} e^{i\alpha_p(C^{(k)}(n)+1)}\frac{2}{C^{(k)}(n)+1} \\ &= e^{\frac{2\pi i}{kp}}\sum_{n=1}^{N=4mp}\frac{(-1)^{\frac{n^2-n}{2p}}}{C^{(k)}(n)+1}. \end{aligned} \tag{26}$$

Where α_p and $C^{(k)}(n)$ were expressed in their functional form as well as expressing $e^{i\pi} = -1$. $\square$

Corollary 7.2. *When $m \to \infty$,*

$$\begin{aligned} I_1 = \frac{e^{\frac{2\pi i}{k}}}{2k\Delta_k}\Bigg[&-\psi\left(\frac{1-\Delta_k}{8}\right)+\psi\left(\frac{3-\Delta_k}{8}\right)+\psi\left(\frac{5-\Delta_k}{8}\right) \\ &-\psi\left(\frac{7-\Delta_k}{8}\right)+\psi\left(\frac{1+\Delta_k}{8}\right)-\psi\left(\frac{3+\Delta_k}{8}\right) \\ &-\psi\left(\frac{5+\Delta_k}{8}\right)+\psi\left(\frac{7+\Delta_k}{8}\right)\Bigg]. \end{aligned} \tag{27}$$

This can also be written as

$$I_1 = \frac{e^{\frac{2\pi i}{k}}}{k\Delta_k}\left[\pi\sec\left(\frac{\pi}{4}(1+\Delta_k)\right)-\pi\csc\left(\frac{\pi}{4}(1+\Delta_k)\right)\right], \tag{28}$$

where ψ is the digamma function [19] and $\Delta_k \equiv \sqrt{\frac{(k-16)}{k}}$.

Proof. When $p = 1$ and $m \to \infty$, Eq. (26) becomes

$$\begin{aligned} I_1 &= \sum_{n=1}^{\infty}\frac{(-1)^{\frac{n^2-n}{2}}}{C^{(k)}(n)+1} = \sum_{n=1}^{\infty}\frac{2(-1)^{\frac{n^2-n}{2}}}{kn^2-kn+4} \\ &= \sum_{n=1}^{\infty}\frac{2(-1)^{\frac{n^2-n}{2}}}{\left(n-\frac{1}{2}+\frac{1}{2}\Delta_k\right)\left(n-\frac{1}{2}-\frac{1}{2}\Delta_k\right)}. \end{aligned} \tag{29}$$

This summation yields to a closed form which is Eq. (27) [19]. Using the relations for the diagamma function built in to MATHEMATICA, this simplifies to Eq. (28) [19]. $\square$

I_1 versus k is shown in Fig. 9. I_1 approaches a k-dependent limit value.

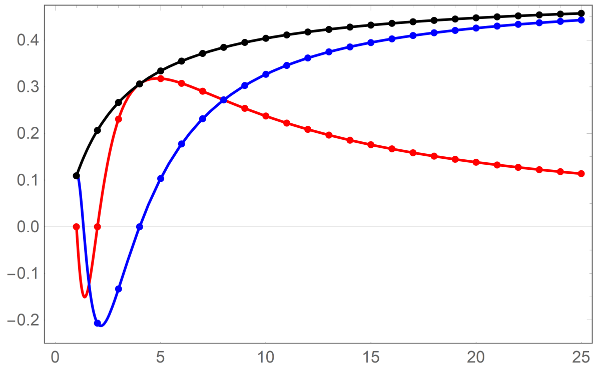

Figure 9. I_1 versus k (dots: $|I_1|$ - black, Re$[I_1]$ - blue, Im$[I_1]$ - red). The curves arise from Eq. (28) in Corollary 7.2.

Corollary 7.3. *On $S^2_{\check{\mathcal{P}}}$, when $m \to \infty$,*

$$I_\infty = \frac{2\pi \tan\left(\frac{1}{2}\pi\Delta_k\right)}{k\Delta_k}, \tag{30}$$

where $\Delta_k \equiv \sqrt{\frac{(k-16)}{k}}$.

Proof. When $p \to \infty$ and $m \to \infty$, Eq. (26) becomes

$$I_\infty = \sum_{n=1}^{\infty} \frac{1}{C^{(k)}(n)+1} = \sum_{n=1}^{\infty} \frac{2}{kn^2 - kn + 4}$$
$$= \sum_{n=1}^{\infty} \frac{2}{\left(n - \frac{1}{2} + \frac{1}{2}\Delta_k\right)\left(n - \frac{1}{2} - \frac{1}{2}\Delta_k\right)}. \tag{31}$$

This summation yields to a closed form which is [19]

$$I_\infty = \frac{2\pi \tan\left(\frac{1}{2}\pi\Delta_k\right)}{k\Delta_k}. \tag{32}$$

This completes the proof. □

Corollary 7.4. $\lim_{k\to\infty} I_1 = \frac{1}{2} = \lim_{k\to\infty} I_\infty$.

Proof. The proof follows from Eq. (28) by L'Hospital's rule. □

Based on Corollary 7.4 the following unproven conjecture is proposed.

Conjecture 7.5. $\lim_{k\to\infty} I_p = \frac{1}{2}$.

As a side-note, $k = 16$ is special and Eqs. (28) and (30) must be evaluated using limits of $k \to 16$ and L'Hospital's rule. When $k = 16$, Eq. (28) becomes $I_1 = \frac{\sqrt[8]{-1}\pi^2}{16\sqrt{2}}$ and Eq. (30) becomes $I_\infty = \frac{\pi^2}{16}$

The closed-loop integral is then on $S^2_{\mathcal{P}}$ and $S^2_{\check{\mathcal{P}}}$,

$$L_{ij} \equiv I_i - I_j. \tag{33}$$

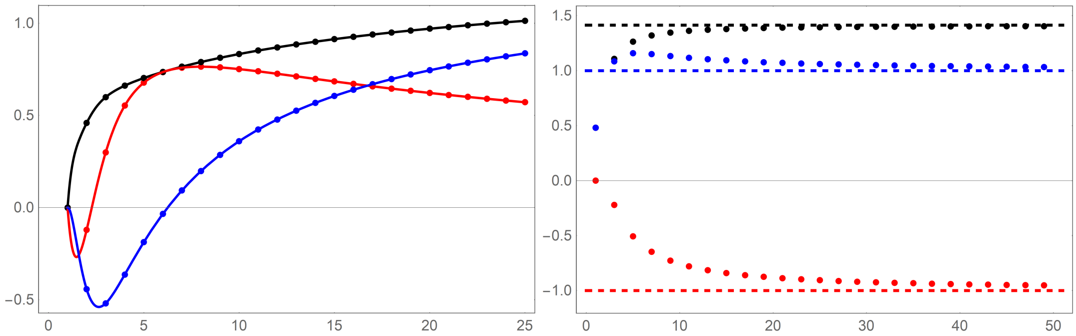

Figure 10. Left Panel: L_{p1} versus p (dots: $|L_{p1}|$ - black, $\mathrm{Re}[L_{p1}]$ - blue, $\mathrm{Im}[L_{p1}]$ - red) for the case of $k = 1$. The curves arise from Eq. (28) in Corollary 7.2. Right Panel: $\frac{k}{\pi}L_{\infty 1}$ versus k ($|\frac{k}{\pi}L_{\infty 1}|$ - black, $\mathrm{Re}[\frac{k}{\pi}L_{\infty 1}]$ - blue, $\mathrm{Im}[\frac{k}{\pi}L_{\infty 1}]$ - red). The dashed lines represent the $\lim_{k\to\infty}\frac{k}{\pi}L_{\infty 1} = 1 - i$.

Of special interest is L_{p1}, where the return path is along $-\Gamma_1$. The left panel of Fig. 10 shows the behavior of L_{p1} for $p = 1$ through $p = 20$ and $k = 1$. A finite limiting values is reached for $L_{\infty 1} \equiv \lim_{p\to\infty} L_{p1}$. It is natural to consider a normalized version of $L_{\infty 1}$ to compare different values of k. This is done by multiplying by $\frac{k}{\pi}$ and a graph is shown in the right panel of Fig. 10. The dashed line in the figure represent the limiting value of $\frac{k}{\pi}L_{\infty 1}$ as $k \to \infty$ as given by the following theorem.

Theorem 7.6. *On $S^2_{\check{\mathcal{P}}}$,*

$$\lim_{k\to\infty} \frac{k}{\pi} L_{\infty 1} = 1 - i \tag{34}$$

Proof. One considers

$$\lim_{k\to\infty} \frac{k}{\pi}(I_\infty - I_1), \tag{35}$$

(*c.f.*, Eqs. (28) and (30)) which upon L'Hospital's rule leads to $1 - i$. □

8. Conclusions

This work focused on the centered polygonal lacunary functions restricted to symmetry angle space. The periodicity of the p-sequences and the existence of a convergent subsequence provided a framework for decomposition of the centered polygonal lacunary functions. This decomposition could be potentially useful in renormalization proceedures as one approaches the natural boundary.

The surjective spherical mapping of the unit disk such that the natural boundary is mapped to the south pole was useful in investigating line integrals of the centered polygonal lacunary functions. Closed form functional representations were achieved in some cases.

It is hoped that this work provides useful insight into the nature of the natural boundary of centered polygonal lacunary functions, both on the full unit disk and also restricted to symmetry angle space.

Author Contributions: L.K.M., K.S. and D.J.U. conceived of and designed the investigation; K.S. and D.J.U. provided background for the investigation; D.J.U. wrote the MATHEMATICA code to perform the investigation; L.K.M., K.S., and D.J.U analyzed the data; D.J.U. wrote the original draft of manuscript; L.K.M., K.S. and D.J.U. edited the manuscript.

Funding: This research was funded by the Concordia College Chemistry Endowment Fund.

Acknowledgments: Douglas R. Anderson, Trenton Vogt and Drew Rutherford are acknowledged for valuable discussion.

Conflicts of Interest: The authors declare no conflict of interest. The funders had no role in the design of the study; in the collection, analyses, or interpretation of data; in the writing of the manuscript, or in the decision to publish the results'.

References

1. Hille, E. *Analytic function theory, Vol. I*. Publisher: Ginn and Company, Boston, MA, 1959.
2. Hille, E. *Analytic function theory, Vol. II*. Publisher: Ginn and Company, Boston, MA, 1962.
3. Shudo, A.; Ikeda, K.S. Tunneling effect and the natural boundary of invariant tori. *Phys. Rev. Lett.* **2012**, 109.
4. Yamada, H.S.; Ikeda, K.S. Analyticity of quantum states in one-dimen-sional tight-binding model. *Eur. Phys. J. B* **2014**, 87, 208.
5. Creagh, S.C.; White, M.M. Evanescent escape from the dielectric ellipse. *J. Phys. A* **2010**, 43, 465102.
6. Nickel, B. On the singularity structure of the 2D Ising model susceptibility. *J. Phys. A: Math. Gen.* **1999**, 32, 3889–3906.
7. Guttmann, A.J.; Enting, I.G. Solvability of some statistical mechanical systems. *Phys. Rev. Lett.* **1996**, 76, 344–347.
8. Orrick, W.P.; Nickel, B.G.; Guttmann, A.J.; Perk, J.H.H. Critical behavior of the two-dimensional Ising susceptibility. *Phys. Rev. Lett.* **2001**, 86, 4120–4123.
9. Jensen, G.; Pommerenke, C.; Ramirez, J.M. On the path properties of a lacunary power series. *Proc. Amer. Math. Soc.* **2014**, 142, 1591–1606.
10. Sullivan, K.; Rutherford, D.; Ulness, D.J. Centered polygonal lacunary sequences. *Mathematics* **2019**, 7, 943.
11. Sullivan, K.; Rutherford, D.; Ulness, D.J. Centered polygonal lacunary Graphs: A graph theoretic approach to p-sequences of centered polygonal lacunary functions. *Mathematics* **2019**, 7, 1021.
12. Mork, L.K.; Vogt, T.; Sullivan, K.; Rutherford, D.; Ulness, D.J. Exploration of filled-in Julia sets arising from centered polygonal lacunary functions. *Fract. and Fract.* **2019**, 3(3), 42.
13. Steen, L.A.; Seebach Jr., J.A. *Counterexamples in topology* Publisher: Dover Publications, New York, 1995.
14. Schlicker, S.J. Numbers simultaneously polygonal and centered polygonal. *Math. Mag.* **2011**, 84, 339–350.
15. Teo, B.K.; Sloane, J.A. Magic numbers in polygonal clusters. *Inorg. Chem.* **1985**, 24, 4545–4558.
16. Deza, E.; Deza, M-M. *Figurate numbers*. Publisher: World Scientific, New Jersey, 2012.
17. Edgar, T. Visual decompositions of polygonal number. *The College Math. J.* **2020**, 51, 9–12.
18. Hoggatt Jr., V. E.; Bicknell, M. Triangular Numbers. *Fibonacci Quarterly* **1974**, 12, 221–230.
19. MATHEMATICA 11. Wolfram Research (2018).